PAPER • OPEN ACCESS

Ultrafast photocurrents in MoSe$_2$ probed by terahertz spectroscopy

View the article online for updates and enhancements.

2D Materials

PAPER

Ultrafast photocurrents in MoSe₂ probed by terahertz spectroscopy

Denis Yagodkin[1] , Lukáš Nádvorník[2,3,4] , Oliver Gueckstock[1,2] , Cornelius Gahl[1] ,
Tobias Kampfrath[1,2] and Kirill I Bolotin[1]

1 Department of Physics, Freie Universität Berlin, Berlin, Germany
2 Department of Physical Chemistry, Fritz Haber Institute of the Max Planck Society, Berlin, Germany
3 Faculty of Mathematics and Physics, Charles University, Prague, Czechia
4 The first two authors contributed equally.

E-mail: iagodkin@zedat.fu-berlin.de and kirill.bolotin@fu-berlin.de

Abstract

We use the terahertz (THz) emission spectroscopy to study femtosecond photocurrent dynamics in the prototypical 2D semiconductor, transition metal dichalcogenide MoSe₂. We identify several distinct mechanisms producing THz radiation in response to an ultrashort (30 fs) optical excitation in a bilayer (BL) and a multilayer (ML) sample. In the ML, the THz radiation is generated at a picosecond timescale by out-of-plane currents due to the drift of photoexcited charge carriers in the surface electric field. The BL emission is generated by an in-plane shift current. Finally, we observe oscillations at about 23 THz in the emission from the BL sample. We attribute the oscillations to quantum beats between two excitonic states with energetic separation of ~100 meV.

Photoinduced carrier dynamics in semiconducting transition metal dichalcogenides (TMDCs) such as MoSe₂, MoS₂, or WSe₂ have been actively investigated recently [1–3]. The dynamics is especially interesting as optical excitations in TMDCs are dominated by excitons, strongly bound electron/hole complexes [4, 5]. Weak screening of excitons leads to large binding energies up to hundreds of meV, making them stable at room temperature [6–9]. Rich dynamics have been shown to result from the interactions between free carriers, neutral excitons, and charged excitons (three-particle complexes) [10–12]. In addition, monolayer TMDCs are two-dimensional materials which can be stacked into heterostructures [13]. The dynamics of interlayer excitons (hole in one layer and electron in another) in such systems can be controlled by the choice of materials [14, 15], stacking parameters [16], and out-of-plane electrical fields [17, 18].

Most of the studies mentioned above use time-resolved absorption/reflection spectroscopies to probe the dynamics of photoexcited carriers. While a wealth of results has been obtained, these techniques have limitations. For example, it is challenging to resolve the out-of-plane dynamics of a photocurrent. Recently, terahertz (THz) emission spectroscopy has emerged as a useful tool to probe ultrafast current dynamics in thin structures [19–21]. In this approach, an ultrafast optical pump pulse is used to excite a photocurrent in the sample. The photocurrent causes the emission of electromagnetic radiation. Duration, direction, and amplitude of this photocurrent define the waveform and amplitude of the radiation which is detected by electro-optic sampling (EOS). The advantages of the approach include the high time resolution [22], excellent sensitivity [23], and the ability to detect both in- and out-of-plane currents [24].

Here, we use THz emission spectroscopy with a very fine time resolution of ~30 fs to study photocurrents in the prototypical TMDC MoSe₂. This time resolution allows us to observe phenomena on time scales that have not been accessible before in TMDCs. We disentangle the dynamics of in-plane and out-of-plane photocurrents by comparing bilayer (BL) and multilayer (ML) MoSe₂ samples and by varying the detection angle. Following photoexcitation, we find relatively slow (time scale ~0.6 ps)
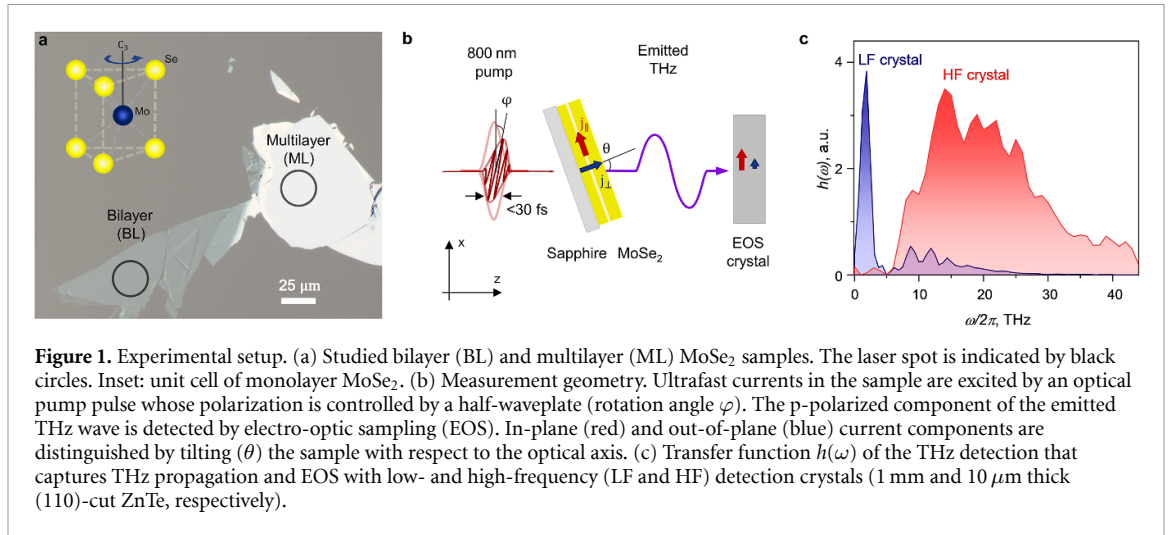
Figure 1. Experimental setup. (a) Studied bilayer (BL) and multilayer (ML) MoSe$_2$ samples. The laser spot is indicated by black circles. Inset: unit cell of monolayer MoSe$_2$. (b) Measurement geometry. Ultrafast currents in the sample are excited by an optical pump pulse whose polarization is controlled by a half-waveplate (rotation angle φ). The p-polarized component of the emitted THz wave is detected by electro-optic sampling (EOS). In-plane (red) and out-of-plane (blue) current components are distinguished by tilting (θ) the sample with respect to the optical axis. (c) Transfer function $h(\omega)$ of the THz detection that captures THz propagation and EOS with low- and high-frequency (LF and HF) detection crystals (1 mm and 10 μm thick (110)-cut ZnTe, respectively).

out-of-plane photocurrents that are dominant in the ML samples and fast ($\sim$50 fs) in-plane photocurrents that are dominant in the BL devices. We ascribe the out-of-plane photocurrent in the ML to drift of photoexcited carriers in the surface electric field [25–28] and the in-plane photocurrent in the BL to a resonant shift current [29–33]. Finally, the large bandwidth of our experiment allows us to detect oscillations in the THz emission which we attribute to quantum beats between inter- and intra-layer excitonic states in MoSe$_2$ [34–36].
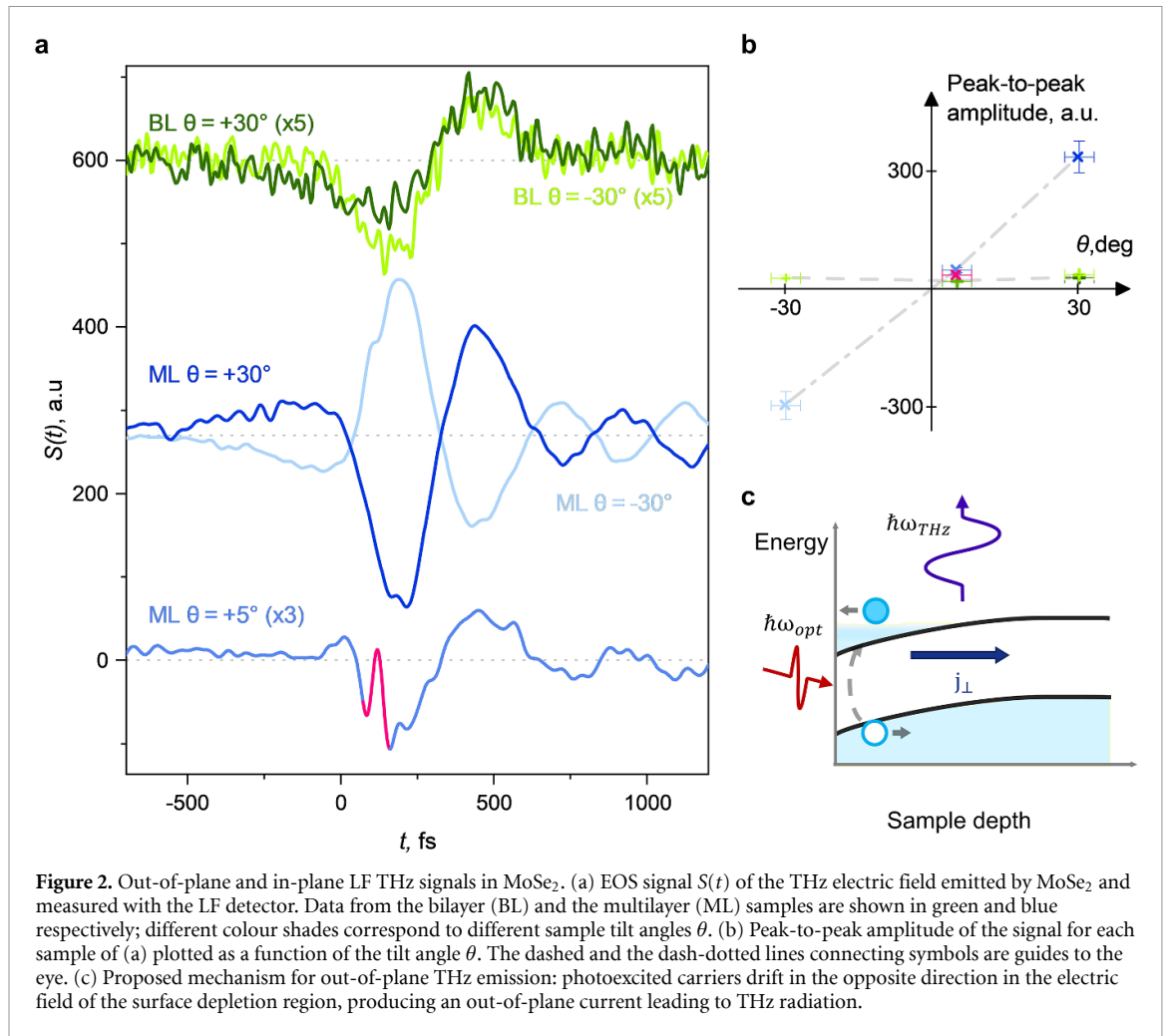
1. Setup

As TMDC sample material, we choose molybdenum diselenide (MoSe$_2$). This material has been shown to have a small density of defects and sharp excitonic peaks [37]. Moreover, its absorption peak is located at $\sim$800 nm [38], close to the emission peak of the used Ti:Sapphire ultrafast laser system. At the same time, the material is representative of the entire TMDC family. To study in- and out-of-plane processes in TMDCs, we exfoliated large-area ($> 40 \times 40\,\mu$m^2) bilayer (BL) and 52 nm-thick (figure S1 (available online at stacks.iop.org/2DM/8/025012/mmedia)) multilayer (ML) MoSe$_2$ samples from bulk crystal (2H-phase) onto a transparent c-cut sapphire substrate (figure 1(a)). Samples were annealed in vacuum at 200 °C and characterized using atomic force microscopy (figure S2) and photoluminescence spectroscopy (figure S3).

In our measurement setup, the laser-induced photocurrent inside the sample is directly probed by recording the THz radiation generated by this photocurrent using electro-optical sampling (EOS) (figure 1(b)) [39, 40]. The ultrafast laser provides pulses with a width of 30 fs, centered at 780 nm, with a repetition rate of 80 MHz and a pulse energy of 1 nJ at the sample position. The beam is split into pump and sampling beams. A half-waveplate is used to control the polarization of the pump beam which is then focused onto the sample by a parabolic mirror resulting in a spot of $\sim$25 μm diameter (black circle in figure 1(a)). The delay between the pump and the sampling beams is set by a precision delay line [41]. The emitted THz radiation arising from pump excitation is focused onto a (110)-cut 1 mm or 10 μm thick ZnTe crystal and overlapped with the focused sampling beam. In the EOS process, the initially linearly polarized sampling pulse acquires an ellipticity that is detected using a quarter-waveplate, a polarizing beamsplitter and balanced photodiodes, resulting in the EOS signal $S(t)$ that scales linearly with the p-polarized component of the THz electric field waveform. Since only the current component perpendicular to the propagation vector of the pump beam (z-axis figure 1(b)) emits the detected THz field, we can distinguish between the current projections in and out of the sample plane ($j_\parallel$ and $j_\perp$) by varying the sample tilt angle θ (figure 1(b)).

In our measurement scheme, the spectral sensitivity of the EOS detection strongly depends on the thickness of the ZnTe crystal [42]. More precisely, in the frequency domain, the detected EOS signal $S(\omega) = h(\omega)E(\omega)$ is related to the THz electric field $E(\omega)$ just behind the sample through a transfer function $h(\omega)$ which describes the spectral sensitivity of the whole detection process, including the propagation of THz radiation and the detector response (supplementary note 1). In figure 1(c), we show the measured $h(\omega)$ for 1 mm thick (blue curve, termed low frequency (LF)) and 10 μm thick (red curve, termed high frequency (HF)) ZnTe detection crystals. The LF and HF crystals cover the spectral ranges 0.8–2.5 and 10–30 THz, respectively.

Experimental data for LF and HF detection are shown in figures 2 and 3, respectively. We first consider the LF data that are dominant in thick multilayer TMDCs before turning our attention to HF processes governing the emission of few-layer samples.

Figure 2. Out-of-plane and in-plane LF THz signals in MoSe$_2$. (a) EOS signal $S(t)$ of the THz electric field emitted by MoSe$_2$ and measured with the LF detector. Data from the bilayer (BL) and the multilayer (ML) samples are shown in green and blue respectively; different colour shades correspond to different sample tilt angles θ. (b) Peak-to-peak amplitude of the signal for each sample of (a) plotted as a function of the tilt angle θ. The dashed and the dash-dotted lines connecting symbols are guides to the eye. (c) Proposed mechanism for out-of-plane THz emission: photoexcited carriers drift in the opposite direction in the electric field of the surface depletion region, producing an out-of-plane current leading to THz radiation.
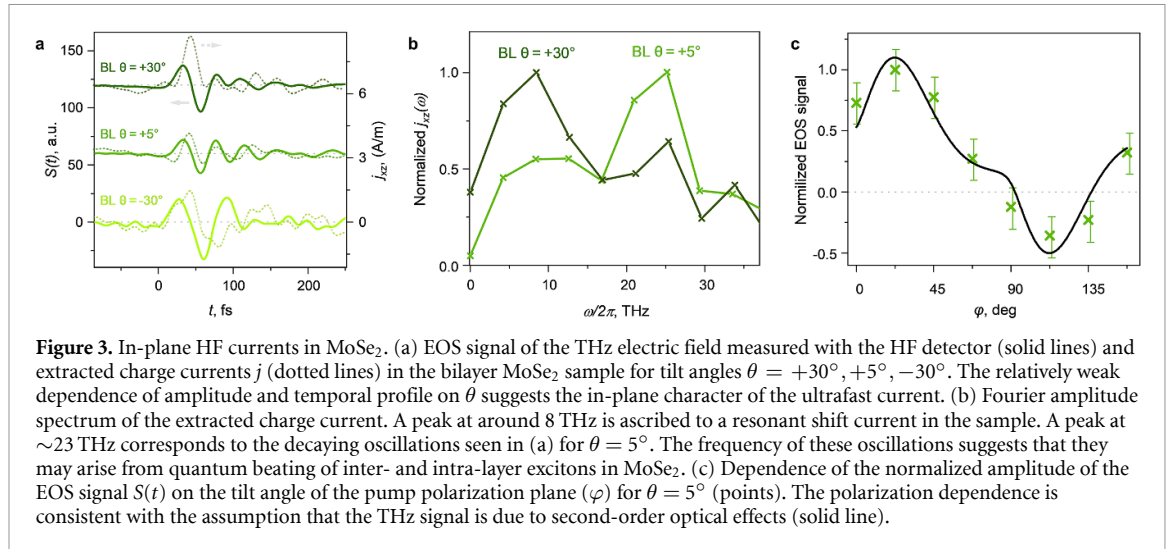
2. Low-frequency THz emission

Figure 2(a) displays a typical EOS signal $S(t)$ of THz pulses emitted by the bilayer region (green) and the multilayer region of the sample (blue) at tilt angles $\theta = +30°, -30°$ and $+5°$ measured with the LF detection crystal. The EOS signal produced by all samples lasts about 500 fs. The residual features seen in figure 2(a) after 500 fs are related to THz excitation and re-emission of residual water vapor [43]. The dependence of the THz signal on the tilt angle θ is different between the ML and the BL (shades of blue and green curves in figure 2(a), respectively, and figure S4). The amplitude and the shape of the emission from the BL sample are similar for tilt angles $\theta = +30°, -30°$, and $+5°$ (for angles close to $0°$, the back-reflected pump affect the laser mode-locking). In contrast, the emission from the ML flips its sign, while maintaining its amplitude, between $\theta = +30°$ and $-30°$. For $\theta = 5°$, the ML signal is strongly reduced (note the scale factor of 3 in figure 2(a)). In addition, a high-frequency feature becomes apparent in the signal at $t \approx 0$ (pink trace in figure 2(a)). The broad spectrum (5–20 THz) of this feature

(figure S5) coincides with spectral regions where the sensitivity of the LF crystal is low (blue curve in figure 1(c)).

The tilt angle dependence of the peak-to-peak amplitudes of the emitted THz pulse for both ML and BL samples is summarized in figure 2(b). The dependence suggests that the signal in the BL is primarily produced by in-plane photocurrents, whereas the signal in the ML samples predominantly stems from out-of-plane photocurrents. Indeed, in-plane currents $j_\parallel$ should produce a signal proportional to $\cos\theta$ without a change in sign. This matches the observed behavior for the BL sample (green symbols in figure 2(b)). In contrast, THz emission from out-plane currents should be proportional to $\sin\theta$ and therefore vanish at $\theta \approx 0$. This behavior is observed for the ML THz emission (blue symbols in figure 2(b)), except for the sharp feature in figure 2 (pink symbols in figure 2(b), see high-pass filtered data in figure S5). Finally, the fact that the sharp feature in the ML signal (the pink trace in figure 2(a)) persists at $\theta = 5°$ suggests that this feature has an in-plane character. This assignment is also supported by a symmetry analysis (figure S6).

Figure 3. In-plane HF currents in MoSe$_2$. (a) EOS signal of the THz electric field measured with the HF detector (solid lines) and extracted charge currents j (dotted lines) in the bilayer MoSe$_2$ sample for tilt angles $\theta = +30°, +5°, -30°$. The relatively weak dependence of amplitude and temporal profile on θ suggests the in-plane character of the ultrafast current. (b) Fourier amplitude spectrum of the extracted charge current. A peak at around 8 THz is ascribed to a resonant shift current in the sample. A peak at $\sim$23 THz corresponds to the decaying oscillations seen in (a) for $\theta = 5°$. The frequency of these oscillations suggests that they may arise from quantum beating of inter- and intra-layer excitons in MoSe$_2$. (c) Dependence of the normalized amplitude of the EOS signal $S(t)$ on the tilt angle of the pump polarization plane (φ) for $\theta = 5°$ (points). The polarization dependence is consistent with the assumption that the THz signal is due to second-order optical effects (solid line).

What are the origins of the observed in-plane and out-of-plane currents in the multilayer MoSe$_2$? Similar out-of-plane emission has been previously observed in other thick TMDCs and ascribed to a drift of photoexcited charge carriers in the built-in electric field appearing close to the surface of the sample due to the surface charged states (figure 2(c)) [26–28]. Indeed, such a mechanism is out-of-plane, is very weak or absent in the BL sample, and should cause THz emission on a picosecond timescale [44, 45]. We note that the emission from another representative TMDC, multilayer WSe$_2$ has similar amplitude and dynamics (figure S7). This is consistent with measurements of that material by others [28, 20] and suggests that the proposed emission mechanism is generic for the TMDC family. At the first glance, it would appear that the in-plane emission occurs at two different timescales—around 500 fs for the BL (green curves in figure 2(a)) and 50 fs for the ML (the pink trace in figure 2(a)). However, the spectral analysis of the latter fast feature in the ML emission reveals significant contribution from outside of the high-sensitivity frequency region (up to 2.5 THz) of the LF crystal (figure S5). Because of that, we hypothesize that the apparently 'slow' in-plane process in the BL may also originate from an intrinsically 'fast' process. We therefore switch to a HF detection crystal (red in figure 1(c)) to further test this hypothesis.

3. High-frequency THz emission

The emission from MoSe$_2$ measured at tilt angles $\theta = +30°, +5°, -30°$ using the 10 μm thick ZnTe crystal sensitive to high-frequencies is shown in figure 3(a) as solid lines for the BL sample and in figure S8 for the ML sample. The dashed lines in figure 3(a) represent the electrical current $j_{xz}(t)$ inside of the sample extracted from EOS signal $S(t)$ following supplementary note 2. The BL emission

features a bipolar swing followed by decaying oscillations that are analyzed later. The timescale of the swing is approximately 50 fs; its amplitude is similar for all tilt angles $\theta = +30°, +5°, -30°$ (figure 3(a)). This suggests the in-plane current nature of the high-frequency emission in the sample. In the ML samples, the tilt angle dependence is more complex (figure S8), however the EOS signal does not flip sign, which is expected for in-plane generating current. Therefore, the HF emission in all samples has an in-plane origin.

Several distinct physical mechanisms contribute to HF in-plane emission in bilayer MoSe$_2$. From a phenomenological viewpoint, we first note that the currents observed here are non-linear second-order optical effects (SOEs). SOEs are expected to produce emission at a difference frequency $\omega = \omega_1 - \omega_2$, for any two frequencies ω_1 and ω_2 inside the pump pulse spectrum [32, 46]. In the case of our 30 fs-long excitations, we expect the emission with a bandwidth of $\sim$33 THz, the inverse of the pump pulse duration. This is consistent with the experimentally observed bandwidth from $\sim$0.3 THz up to 30 THz in the BL MoSe$_2$ (see figure 3(b) and figure S4 for Fourier transform of green curves in figure 2(a)). The lower amplitude of the HF components in spectrum of the BL emission at $\theta = -30°$ is related to variation in sensitivity of the detection at high frequency. In general, SOEs appear in media which lack inversion symmetry [32, 31]. While even-layered MoSe$_2$ is inversion-symmetric, inversion symmetry is broken in each individual layer of the structure [47] (figure 1(a), Inset). The bending of the MoSe$_2$ band structure at interfaces, responsible for ML emission (figure 2(c)), causes an asymmetry between the top and the bottom layers of the stacks [27, 28, 48, 49]. We obtain further evidence for the contribution of SOEs by analyzing the dependence of the emitted THz from the BL on the polarization angle of the pump pulse φ (figure 3(c)). We observe $\sin(2\varphi)$-like behavior in the emitted signal (points in figure 3(c)),

where φ is the tilt of the polarization plane of the initially p-polarized pump beam. This dependence is expected for SOEs as their efficiency depends on the respective alignment between the electrical field of the pump and crystallographic axes of the sample [24, 32, 50]. In supplementary note 2, we derive an analytical expression for the angle-dependence of the emitted field in the BL MoSe$_2$. A good match of this expression (black line in figure 3(c)) to the experimental data (crosses in figure 3(c)) confirms second-order optical effects as dominant processes.

To discuss the microscopic origins of the photocurrents observed here, we note that, in general, multiple distinct SOE effects may contribute in our samples, the most notable of which are injection currents and shift currents [29–33]. The injection currents are only expected under illumination with circularly polarized light, while we use only linearly polarized pump pulses [32, 46]. The off-resonant shift current (also referred to as 'optical rectification') is expected to generate order of magnitude smaller currents [24, 51] than the remaining SOE mechanism: the resonant shift current. The latter current arises from a spatial shift of the center of mass of the electron density within a unit cell when excited from the valence to the conduction bands [24, 46]. Indeed, the photon energy of the pump pulse (1.51–1.70 eV) is in resonance with excitonic transitions in the BL MoSe$_2$ (1.53 eV, figure S3). Moreover, a swing from positive to negative photocurrent, most prominently seen in figure 3(a) at $\theta = 30°$, is a temporal feature expected from a shift current but not from other SOE mechanisms [24]. Therefore, we assign the THz emission from the BL MoSe$_2$ to the resonant shift current.

We finally address the oscillations in the EOS signal $S(t)$ that are especially prominent in the BL signal at $\theta = 5°$ tilt (figure 3(a) after ∼75 fs). The same feature is evident in the extracted current for bilayer MoSe$_2$ (dashed lines in figure 3(a)).

The spectral content of the oscillations is distinct from that of other types of emission we observed in the ML or the BL samples. The Fourier transform with a narrow square window of 240 fs is shown in figure 3(b) (see the analysis in supplementary figure S9). It features two distinct peaks: a low-frequency (centered around 8 THz) peak, assigned to the resonant shift current considered earlier, and a high-frequency peak (around 23 THz). Note that the transfer function of the used detection scheme (red in figure 1(c)) is flat around the center of this peak. Therefore, this peak is not due to the limited spectral response of the detector. Relative intensity of the high-frequency peak depends on the tilt angle θ and matches visibility of the oscillations.

We suggest that the high frequency (23 ± 3 THz) and fast decay constant of 55 fs (figure S10) of the photocurrent oscillations are related to quantum beats between two states separated by the corresponding energy (95 ± 15 meV) and coherently excited by the pump. This type of emission was first observed with heavy and light hole states in GaAs quantum wells at low temperature [35, 36] and theoretically predicted to be efficient for in-plane and out-of-plane excitons [52–54], which are found in TMDCs [17, 14]. Moreover, quantum beats between anisotropic excitons were recently observed in time-resolved differential transmittance of atomically thin ReS$_2$ TMDCs at low temperature [55]. A pair of excitonic states in the bilayer MoSe$_2$ corresponding to observed quantum beats should (a) fall within the pump spectral bandwidth 1.51–1.70 eV, (b) have the energy separation ∼95 ± 15 meV, (c) different dipole moments, and (d) comparable oscillator strengths. The following excitonic states lie within the bandwidth of the pump: neutral ground state intralayer exciton (A), excited states of this exciton (An), charged exciton (trion T), biexciton (X), and interlayer exciton (I) [56, 57]. Of these, the only states matching the required energy separation is the A–I pair with the energy difference $\Delta E_{A-I} \approx 82$ meV. We note that this energy difference is extrapolated from the low-temperature measurements [57, 58], where these peaks are clearly visible, to room temperature. In addition, the two states A and I have comparable oscillator strengths [57, 58] and different dipole moments, in-plane for A [59] and out-of-plane for I [60]. Finally, the decay time of 55 fs (figure S10) matches the dephasing time for excitonic species extrapolated from low to room temperature [61–63]. Therefore, we propose that quantum beats between intra- and inter-layer excitonic species are related the observed oscillations in THz emission.

To summarize, we observed THz photocurrents in bilayer (BL) and multilayer (ML) MoSe$_2$ in both low-frequency (0.8–2.5 THz) and high-frequency (10–30 THz) spectral regions using ultrafast terahertz emission spectroscopy. The low-frequency emission from the multilayer sample features a radiation pattern typical for an out-of-plane charge flow. We attribute this emission to drift of photogenerated carriers in the surface electric filed. In contrast, the angular distribution of the THz emission from the BL sample is consistent with in-plane photocurrents. By analyzing the polarization dependence and amplitude of this emission at high frequency, we are led to ascribe it to a resonant shift current. Furthermore, THz emission from the BL sample features oscillations of the emitted field. Frequency and decay time of these oscillations are consistent with quantum beats between coherently excited inter- and intra-layer excitons as generation process. Our findings provide a picture of photocurrent processes following ultrafast optical excitation of TMDCs. Finally, quantum beats may enable novel wavelength-tunable room temperature THz emitters

once electrical tunability is demonstrated and THz emission intensity is improved.

Acknowledgments

ORCID iDs

Denis Yagodkin ⬤ https://orcid.org/0000-0002-9135-8918
Lukáš Nádvorník ⬤ https://orcid.org/0000-0002-4469-656X
Oliver Gueckstock ⬤ https://orcid.org/0000-0003-2361-127X
Cornelius Gahl ⬤ https://orcid.org/0000-0002-9833-8581
Tobias Kampfrath ⬤ https://orcid.org/0000-0001-8854-8713
Kirill I Bolotin ⬤ https://orcid.org/0000-0003-1821-3429

References

[1] Amani M *et al* 2015 Near-unity photoluminescence quantum yield in MoS$_2$ *Science* **350** 1065–8
[2] Massicotte M *et al* 2018 Dissociation of two-dimensional excitons in monolayer WSe$_2$ *Nat. Commun.* **9** 1633
[3] Godde T *et al* 2016 Exciton and trion dynamics in atomically thin MoSe$_2$ and WSe$_2$: effect of localization *Phys. Rev. B* **94** 165301
[4] Li Y *et al* 2014 Measurement of the optical dielectric function of monolayer transition-metal dichalcogenides: MoS$_2$, MoSe$_2$, WS$_2$ and WSe$_2$ *Phys. Rev. B* **90** 205422
[5] Klots A R *et al* 2014 Probing excitonic states in suspended two-dimensional semiconductors by photocurrent spectroscopy *Sci. Rep.* **4** 6608
[6] Chernikov A, Berkelbach T C, Hill H M, Rigosi A, Li Y, Aslan O B, Reichman D R, Hybertsen M S and Heinz T F 2014 Exciton binding energy and nonhydrogenic Rydberg series in monolayer WS$_2$ *Phys. Rev. Lett.* **113** 076802
[7] Klots A R, Weintrub B, Prasai D, Kidd D, Varga K, Velizhanin K A and Bolotin K I 2018 Controlled dynamic screening of excitonic complexes in 2D semiconductors *Sci. Rep.* **8** 768
[8] Greben K, Arora S, Harats M G and Bolotin K I 2020 Intrinsic and extrinsic defect-related excitons in TMDCs *Nano Lett.* **20** 2544–50
[9] Poellmann C *et al* 2015 Resonant internal quantum transitions and femtosecond radiative decay of excitons in monolayer WSe$_2$ *Nat. Mater.* **14** 889–93
[10] Singh A *et al* 2016 Trion formation dynamics in monolayer transition metal dichalcogenides *Phys. Rev. B* **93** 041401
[11] Ye J, Yan T, Niu B, Li Y and Zhang X 2018 Nonlinear dynamics of trions under strong optical excitation in monolayer MoSe$_2$ *Sci. Rep.* **8** 2389
[12] Yu Y, Yu Y, Xu C, Barrette A, Gundogdu K and Cao L 2016 Fundamental limits of exciton-exciton annihilation for light emission in transition metal dichalcogenide monolayers *Phys. Rev. B* **93** 201111
[13] Novoselov K S, Mishchenko A, Carvalho A and Castro Neto A H 2016 2D materials and van der Waals heterostructures *Science* **353** 6298
[14] Chen H *et al* 2016 Ultrafast formation of interlayer hot excitons in atomically thin MoS$_2$/WS$_2$ heterostructures *Nat. Commun.* **7** 12512
[15] Hanbicki A T, Chuang H-J, Rosenberger M R, Hellberg C S, Sivaram S V, McCreary K M, Mazin I I and Jonker B T 2018 Double indirect interlayer exciton in a MoSe$_2$/WSe$_2$ van der Waals heterostructure *ACS Nano* **12** 4719–26
[16] Zhu H, Wang J, Gong Z, Kim Y D, Hone J and Zhu X-Y 2017 Interfacial charge transfer circumventing momentum mismatch at two-dimensional van der Waals heterojunctions *Nano Lett.* **17** 3591–8
[17] Rivera P, Seyler K L, Yu H, Schaibley J R, Yan J, Mandrus D G, Yao W and Xu X 2016 Valley-polarized exciton dynamics in a 2D semiconductor heterostructure *Science* **351** 688–91
[18] Jin C, Ma E Y, Karni O, Regan E C, Wang F and Heinz T F 2018 Ultrafast dynamics in van der Waals heterostructures *Nat. Nanotechnol.* **13** 994
[19] Ma E Y, Guzelturk B, Li G, Cao L, Shen Z-X, Lindenberg A M and Heinz T F 2019 Recording interfacial currents on the subnanometer length and femtosecond time scale by terahertz emission *Sci. Adv.* **5** eaau0073
[20] Huang Y, Yao Z, He C, Zhu L, Zhang L, Bai J and Xu X 2019 Terahertz surface and interface emission spectroscopy for advanced materials *J. Phys.: Condens. Matter.* **31** 153001
[21] Stein M, Fuchs C, Stolz W, Mittleman D M and Koch M 2020 Direct probe of room-temperature quantum-tunneling processes in type-II heterostructures using terahertz emission spectroscopy *Phys. Rev. Appl.* **13** 054073
[22] Seifert T S *et al* 2018 Femtosecond formation dynamics of the spin seebeck effect revealed by terahertz spectroscopy *Nat. Commun.* **9** 2899
[23] Porer M, Ménard J-M and Huber R 2014 Shot noise reduced terahertz detection via spectrally postfiltered electro-optic sampling *Opt. Lett.* **39** 2435
[24] Braun L, Mussler G, Hruban A, Konczykowski M, Schumann T, Wolf M, Münzenberg M, Perfetti L and Kampfrath T 2016 Ultrafast photocurrents at the surface of the three-dimensional topological insulator Bi$_2$Se$_3$ *Nat. Commun.* **7** 13259
[25] Zhang X, Hu B B, Darrow J T and Auston D H 1990 Generation of femtosecond electromagnetic pulses from semiconductor surfaces *Appl. Phys. Lett.* **56** 1011
[26] Huang Y, Zhu L, Yao Z, Zhang L, He C, Zhao Q, Bai J and Xu X 2017a Terahertz surface emission from layered MoS$_2$ crystal: competition between surface optical rectification and surface photocurrent surge *J. Phys. Chem. C* **122** 481
[27] Zhang L, Huang Y, Zhao Q, Zhu L, Yao Z, Zhou Y, Du W and Xu X 2017 Terahertz surface emission of d-band electrons from a layered tungsten disulfide crystal by the surface field *Phys. Rev. B* **96** 155202
[28] Si K, Huang Y, Zhao Q, Zhu L, Zhang L, Yao Z and Xu X 2018 Terahertz surface emission from layered semiconductor WSe$_2$ *Appl. Surf. Sci.* **448** 416—423
[29] Zhang X-C, Jin Y, Yang K and Schowalter L J 1992 Resonant nonlinear susceptibility near the GaAs band gap *Phys. Rev. Lett.* **69** 2303–6
[30] Côté D, Laman N and van Driel H M 2002 Rectification and shift currents in GaAs *Appl. Phys. Lett.* **80** 905–7
[31] Sipe J E and Shkrebtii A I 2000 Second-order optical response in semiconductors *Phys. Rev. B* **61** 5337–52
[32] Nastos F and Sipe J E 2006 Optical rectification and shift currents in GaAs and gap response: below and above the band gap *Phys. Rev. B* **74** 035201
[33] Nastos F and Sipe J 2010 Optical rectification and current injection in unbiased semiconductors *Phys. Rev. B* **82** 235204

[34] Göbel E O, Leo K, Damen T C, Shah J, Schmitt-Rink S, Schäfer W, Müller J F and Köhler K 1990 Quantum beats of excitons in quantum wells *Phys. Rev. Lett.* **64** 1801–4

[35] Planken P C, Nuss M C, Brener I, Goossen K W, Luo M S, Chuang S L and Pfeiffer L 1992 Terahertz emission in single quantum wells after coherent optical excitation of light hole and heavy hole excitons *Phys. Rev. Lett.* **69** 3800

[36] Brener I, Planken P C M, Nuss M C, Luo M S C, Chuang S L, Pfeiffer L, Leaird D E and Weiner A M 1994 Coherent control of terahertz emission and carrier populations in semiconductor heterostructures *J. Opt. Soc. Am.* B **11** 2457

[37] Cadiz F *et al* 2017 Excitonic linewidth approaching the homogeneous limit in MoS_2-based van der Waals heterostructures *Phys. Rev. X* **7** 021026

[38] Tonndorf P *et al* 2013 Photoluminescence emission and Raman response of monolayer MoS_2, $MoSe_2$ and WSe_2 *Opt. Express* **21** 4908

[39] Seifert T S 2017 Spintronics with terahertz radiation: probing and driving spins at highest frequencies PhD Thesis School Freie Universität Berlin, Berlin

[40] Kampfrath T, Nötzold J and Wolf M 2007 Sampling of broadband terahertz pulses with thick electro-optic crystals *Appl. Phys. Lett.* **90** 231113

[41] Shimada T, Kamaraju N, Frischkorn C, Wolf M and Kampfrath T 2014 Indication of Te segregation in laser-irradiated ZnTe observed by *in situ* coherent-phonon spectroscopy *Appl. Phys. Lett.* **105** 111908

[42] Zhao Z, Schwagmann A, Ospald F, Driscoll D C, Lu H, Gossard A C and Smet J H 2010 Thickness dependence of the terahertz response in 110-oriented GaAs crystals for electro-optic sampling at 155 μm *Opt. Express* **18** 15956

[43] Beck M, Schäfer H, Klatt G, Demsar J, Winnerl S, Helm M and Dekorsy T 2010 Impulsive terahertz radiation with high electric fields from an amplifier-driven large-area photoconductive antenna *Opt. Express* **18** 9251

[44] Johnston M B, Whittaker D M, Corchia A, Davies A G and Linfield E H 2002 Simulation of terahertz generation at semiconductor surfaces *Phys. Rev. B* **65** 165301

[45] Heyman J N, Coates N, Reinhardt A and Strasser G 2003 Diffusion and drift in terahertz emission at GaAs surfaces *Appl. Phys. Lett.* **83** 5476–8

[46] Fregoso B M 2019 Bulk photovoltaic effects in the presence of a static electric field *Phys. Rev. B* **100** 064301

[47] Manzeli S, Ovchinnikov D, Pasquier D, Yazyev O V and Kis A 2017 2D transition metal dichalcogenides *Nat. Rev. Mater.* **2** 17033

[48] Steinberg H, Gardner D R, Lee Y S and Jarillo-Herrero P 2010 Surface state transport and ambipolar electric field effect in Bi_2Se_3 nanodevices *Nano Lett.* **10** 5032–6

[49] McIver J W, Hsieh D, Drapcho S G, Torchinsky D H, Gardner D R, Lee Y S and Gedik N 2012 Theoretical and experimental study of second harmonic generation from the surface of the topological insulator Bi_2Se_3 *Phys. Rev. B* **86** 035327

[50] Huang Y, Zhu L, Zhao Q, Guo Y, Ren Z, Bai J and Xu X 2017b Surface optical rectification from layered MoS_2 crystal by THz time-domain surface emission spectroscopy *ACS Appl. Mater. Interfaces* **9** 4956–65

[51] Ferguson B and Zhang X-C 2002 Materials for terahertz science and technology *Nat. Mater.* **1** 26–33

[52] Kyriienko O, Kavokin A and Shelykh I 2013 Superradiant terahertz emission by dipolaritons *Phys. Rev. Lett.* **111** 176401

[53] Kristinsson K, Kyriienko O, Liew T C H and Shelykh I A 2013 Continuous terahertz emission from dipolaritons *Phys. Rev. B* **88** 245303

[54] Kristinsson K, Kyriienko O and Shelykh I 2014 Terahertz laser based on dipolaritons *Phys. Rev. A* **89** 023836

[55] Sim S *et al* 2018 Ultrafast quantum beats of anisotropic excitons in atomically thin ReS_2 *Nat. Commun.* **9** 351

[56] Pei J *et al* 2017 Excited state biexcitons in atomically thin $MoSe_2$ *ACS Nano* **11** 7468–75

[57] Horng J, Stroucken T, Zhang L, Paik E Y, Deng H and Koch S W 2018 Observation of interlayer excitons in $MoSe_2$ single crystals *Phys. Rev. B* **97** 241404

[58] Gerber I C *et al* 2019 Interlayer excitons in bilayer MoS_2 with strong oscillator strength up to room temperature *Phys. Rev. B* **99** 035443

[59] Schuller J A, Karaveli S, Schiros T, He K, Yang S, Kymissis I, Shan J and Zia R 2013 Orientation of luminescent excitons in layered nanomaterials *Nat. Nanotechnol.* **8** 271

[60] Wang Z, Chiu Y-H, Honz K, Mak K F and Shan J 2017 Electrical tuning of interlayer exciton gases in WSe_2 bilayers *Nano Lett.* **18** 137

[61] Jakubczyk T, Delmonte V, Koperski M, Nogajewski K, Faugeras C, Langbein W, Potemski M and Kasprzak J 2016 Radiatively limited dephasing and exciton dynamics in $MoSe_2$ monolayers revealed with four-wave mixing microscopy *Nano Lett.* **16** 5333–9

[62] Shepard G D, Ardelean J V, Ajayi O A, Rhodes D, Zhu X, Hone J C and Strauf S 2017 Trion-species-resolved quantum beats in $MoSe_2$ *ACS Nano* **11** 11550–8

[63] Moody G *et al* 2015 Intrinsic homogeneous linewidth and broadening mechanisms of excitons in monolayer transition metal dichalcogenides *Nat. Commun.* **6** 8315